Send Orders for Reprints to reprints@benthamscience.ae

Current Nanoscience, **2015,** *11,* **263-270**

Theoretical Calculation of the Local Heating Effect on the Crystallization of TiO_2 Prepared by Sparking Anodization

M.S. Sikora[1,3], J. Carstensen[2], H. Föll[2] and E.C. Pereira*[3]

[1]*UTFPR, Via do Conhecimento Km 01, 85503-390, P.O. Box 571, Pato Branco, Brazil;* [2]*Institute for Materials Science, Christian-Albrechts-University of Kiel, Kaiserstrasse 2, 24143 Kiel, Germany;* [3]*Interdisciplinary Laboratory of Electrochemistry and Ceramics (LIEC), DQ, UFSCar, P.O. Box: 676, 13565-905, São Carlos, Brazil*

E.C. Pereira

Abstract: Sparks are frequently observed during dielectric breakdown on valve metal oxide films, and several papers investigated their correlation with the oxide crystallization. In this work, the effect of high temperature of a spark was studied using finite element method. An important result is that the oxide area heated above the oxide fusion temperature is more than 50 times larger than the diameter of the channel generated during the breakdown event, meaning that just a few numbers of sparks could lead to a large area of oxide crystallization. Besides, the heated area is proportional to the spark temperature and to the oxide thickness. Finally, using a factorial design, a cross effect was also detected between the channel temperature and the barrier oxide thickness.

Keywords: Computer modeling and simulation, electrochemical properties, finite element analysis, oxides, thin films.

INTRODUCTION

Titanium and Titanium alloys are widely used in several branches of industry, such as aerospace [1, 2], textile [1], electronic [1], automotive [1] and biomedical [3-7], due to their high corrosion resistance and compatibility with human tissue. An improvement in the results of these applications is achieved when the metal or metal alloys are coated with an oxide layer. Such coating process decreases the friction coefficient and also increases the wear [1, 8] and heat resistance [1] of the final material.

Among those techniques employed to coat metals, sparking anodization, also referred as plasma electrolytic oxidation (PEO) [1, 9-13], has been extensively used to synthesize oxide coatings over titanium. Sparking anodization can be carried out through the application of either a constant current or voltage in the working electrode. During the process, localized electrical discharges, known as sparks, glow or mircro-arc, can be observed on the surface of the working electrode [11-15], which are, according to several authors [16-20], consequences of the local dielectric breakdown of the oxide film. The properties of the films prepared by this technique are strongly influenced by the experimental conditions. For example, their morphology can show a wide range of characteristics, such as, homogeneous surface, non-homogeneous surface with pores [9, 21], or, under special conditions, partial crystallization [9, 22]. Concerning this last property, in the past few years, the cause of the crystallization was extensively discussed in the literature. There were two different theories to explain this phenomenon [23-26]. According to the first one, the crystallization of the films could be attributed to the compressive stress accumulated during the oxide growth [23], which is a quite plausible proposal since the electrical field generated during the growth of a barrier layer without any pores is about 10^6-10^7 V cm^{-1}. However, this hypothesis can only describe compact layers and is not valid for porous films. The growth of porous films presents less resistive paths, so the current is localized, and therefore its average value cannot be used to describe the process.

The second theory assumes that an effect of the dielectric breakdown, which is the increase in the local temperature, is responsible for the conversion of amorphous oxide into a crystalline one. This theory was recently supported by measurements of the local temperature during micro-discharge events. Several research groups have shown through optical emission spectroscopy that the micro-discharges can reach extremely high temperatures in the range from 3000-16000 K [21, 26-28], which is high enough to crystallize the amorphous oxide.

Recently, Houser and Herbert [29] published a model about the growth of nanoporous alumina using the hypothesis that the viscous flow originated by the stress of growing oxide is the main factor responsible for the morphological structure changes that are experimentally observed. According to those authors, the stress originated in the oxide growth is released as newtonian viscous flow. Even though a migration transport should not describe the growth mechanism where pores are observed, in that work, the authors demonstrated the existence of a viscous flow during the growth of the oxide. This model, however, disregards the variation of the local thickness of the barrier film and hence also neglects

*Address correspondence to this author at the Interdisciplinary Laboratory of Electrochemistry and Ceramics (LIEC), DQ, UFSCar, P.O. Box: 676, 13565-905, São Carlos, Brazil; Tel: +55 16 3351 9309;
Fax: + 55 16 3351 8214; E-mail: ernesto@ufscar.br

1875-6786/15 $58.00+.00

the fluctuations in the applied electrical field. Therefore, it seems that, despite the great result obtained, the main supposition of the model fails when considering that the porous structure is formed by migration.

The breakdown is a localized event which leads to the formation of a channel in the oxide film as well as the emission of a spark. When the dielectric breakdown is assumed to be the cause of the observed sparks, it is implicit that the high local electrical field is responsible for the breakdown of the film. Consequently, the internal energy of the oxide is released as heat to the surroundings and the open free resistance channel formed is the preferred path for the current. Therefore, this energy released can be measured by the variation of local temperature in the oxide. According to Diamantini and Pedeferri [26], the temperature of sparks is high enough to promote the melting of the solid phases (oxide and metal) in the surrounding region of a spark event.

Based on the previous papers [1, 12, 14, 30-32] the aim of the present work is to contribute to the explanation of the relationship between the dielectric breakdown and crystallization process, studying the influence of the temperature on the surroundings of the spark channel solving the Fourier's equation by finite element method using titanium sparking anodization as model.

PROCEDURES

1. Experimental

To prepare titanium oxide films by sparking anodization technique, a titanium plate (Alfa Aesar 99.5%) of 0.25 mm thickness with 1 cm^2 area was used as working electrode and two platinum plates symmetrically positioned at the titanium electrode were used as counter electrodes. The films were prepared in H_3PO_4 0.3 mol L^{-1} aqueous solution using a constant current density of 20 mA cm^{-2} applied by a high voltage and low current homemade current source measuring the potential difference between working electrode and counter electrode with an HP® 34410A multimeter coupled with a computer by a homemade program routine using the HP-VEE® 5.0 software. The samples were prepared using different charges in the range of 1.8 to 216 C.

The temperature of the bulk of the aqueous solution was maintained constant at 20°C using a Nova Etica HX 521/4D thermostat/cryostat. The crystalline characteristics were investigated using an X-ray diffraction (XRD) Rigaku D/max 2500 PC diffractometer with Cu Kα=1.5406 Å radiation at 40 kV and 150 mA. The diffraction patterns were analyzed using the Rietveld Refinement.

2. Simulation

The equations were solved by Finite Element Method using the COMSOL Multiphysics software [33], version 4.0a, which is a general purpose finite element software. The calculations were run in a PC with 2.8 GHz processor intel i7 and 16Gb of RAM.

Model Development

In a published paper [22], we have found that the sparking anodization process promotes the crystallization of the film (just anatase phase was observed in that specific growth condition). In Fig. (**1**), the signed region, which corresponds to the main peak of anatase phase (101), shows that the crystalline portion of the titanium oxide increases in the course of the anodization process. The (A) XRD pattern is from a pure titanium electrode; when the experiments starts a constant current density is imposed to the metal and the oxide grows, and the rise of the peak referring to anatase phase, which is proportional to the applied charge is noticed. As discussed in that paper [22], the thickness can be considered as a function of the applied charge and the voltage attained during the sample anodization. In addition, this conclusion can be extended to the conversion of amorphous titanium oxide to the anatase one. This argument can be supported by the new experimental observations of an intensification of a spark, bright to naked eye from the beginning to the end of the film preparation, as shown in Fig. (**2b** and **c**). The intensification of sparks means more energy released in a smaller region, consequently the heating of the oxide over the fusion temperature is higher, so more crystalline oxide is formed.

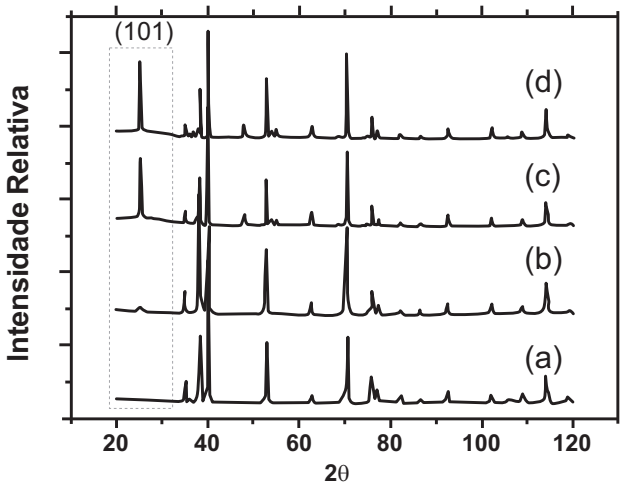

Fig. (1). XRD patterns of (a) pure titanium sample and TiO_2 samples obtained after application of (b) 4.6 C, (c) 25 C and (d) 72 C.

Thus, one possible explanation for the crystallization of the film would be the heat dissipated by each event of breakdown. Once we consider the sparks as a direct result of the film breakdown, in thick films they become more apparent, probably because the energy released in the breakdown of the thick films is higher than the energy released during the breakdown of thin oxide films. These experimental facts are the origin of the present work, where different experimental conditions were explored using computational experiments in order to verify if the hypothesis of crystallization by heat dissipation in each event of breakdown would be reasonable or not.

In order to simulate the effect of the spark on the titanium oxide films it is necessary to present a theoretical model to describe the growth mechanism of titanium oxide under sparking anodization conditions.

In the beginning of an anodization experiment, the oxide grows due to ionic migration [18, 34]. As consequence, an

increase in the voltage is necessary to sustain the current flux at a constant value, as can be seen in the anodization curve shown in Fig. (**2**). After that, due to the high voltage applied to the oxide, the electrical field inside the film reaches a critical value for dielectric breakdown to occur and as consequence, voltage oscillations in the anodization curve (Fig. **2**) are observed. Different papers propose a change in the growth mechanism, where both ionic and electronic current assume an important role [16, 18]. In this region, the local breakdown event (electronic) destroys the oxide film at a specific point. As a side effect of the local breakdown, sparks can be observed over the surface of the titanium electrode, as shown in Fig. (**2**) at the right.

Once the channel is open due to the breakdown event, the charge carriers have a preferred path with zero resistance to current flow. Therefore, the migration mechanism is no longer successful to describe the film formation after the breakdown begins. In the present work we have used the same arguments utilized in the current burst model (CBM) [35-38] to describe the initiation of the sparking anodization, which is briefly reported below. In the CBM, the charge transfer occurs only in the regions where the breakdown is active.

In this case the electrical field is given by $= \frac{U}{S}$. Even in those cases where the film has two components: a barrier and a porous layer, this model is valid since the most important part is the barrier layer, i.e., the following approximation is valid:

$$E = \frac{U}{s} = \frac{U_0 - R_p I}{s_b} = \frac{U_b}{s_b} \quad (1)$$

Where U_0 is the applied voltage, R_p is the resistance of the porous layer, I is the applied current and s_b is the thickness of the barrier layer. This equation means that, even with the porous layer, the breakdown phenomena always occurs in the barrier layer because the voltage drop in the porous layer is insignificant.

In the present work, only one spark event in the barrier layer will be considered in order to decrease the computational effort. The Fourier equation was solved by finite element method (FEM) in order to simulate the spark effect on its surroundings. The application of FEM is based on the modeling of the domain through its division in an equivalent system but with smaller units, which are called finite elements. These elements are connected by common points, between two or more elements, which are called nodes [39]. The formulation of the problem using finite elements results in a system with simultaneous solutions of algebraic equations instead of solving the overall differential equations of the domain.

As domain for this simulation, we have considered the three media involved: metal, oxide and electrolyte, as presented in Fig. (**3**). The domain represents a small region of the electrode that is in contact with the solution. We have also considered the system's dimension, i.e, we have not used a dimensionless approach which is very common in computational experiments. This decision is based on the fact that the system´s size is important to follow the extension of the effects on the surroundings of a spark.

When considering all the parts of a sparking anodization system, the gas phase should be included, once the solution next to the channel passes from the liquid phase to the gaseous one due to the high local temperature. However, in a simulation work, simplifications must be made to minimize the computational effort. Thus, we disregard the gaseous phase, once it detaches quickly from the surface of the electrode and is replaced by electrolytic solution.

In the first frame of Fig. (**3**) the complete domain is shown. It was considered that the oxide has 100 μm of thickness with a symmetric pore with no ramification. The main objective of this investigation is to comprehend how the heat released by a 'one spark' event can affect the properties of the films. To accomplish this, a pore with a diameter of 1 μm was proposed, in agreement to experimental results obtained previously by scanning electron microscopy [22].

The encircled region in the frame A of Fig. (**3**) is presented amplified in frame B. In this frame the pore region and the interface between the oxide and the solution is presented, which is marked as C. In this last subregion, the oxide layer that separates the metal from the solution is smaller by many orders of magnitude compared to the thick oxide without pores.

Inasmuch as the breakdown occurs and considering that the electrical field is inversely proportional to the thickness

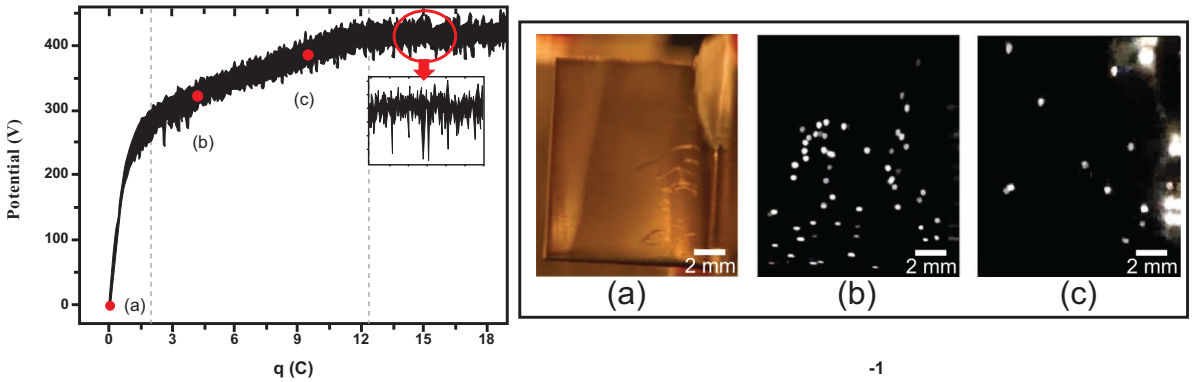

Fig. (2). Sparking anodization curve for titanium in 0.3 mol L^{-1} phosphoric acid solution, 20°C and applying 20 mA cm^{-2}. At right: sparks on the surface of the titanium electrode during the sparking anodization process at: (**a**) titanium electrode before the anodization. (**b**) and (**c**) Sparks on the electrode surface at indicated points in the voltage x charge curve.

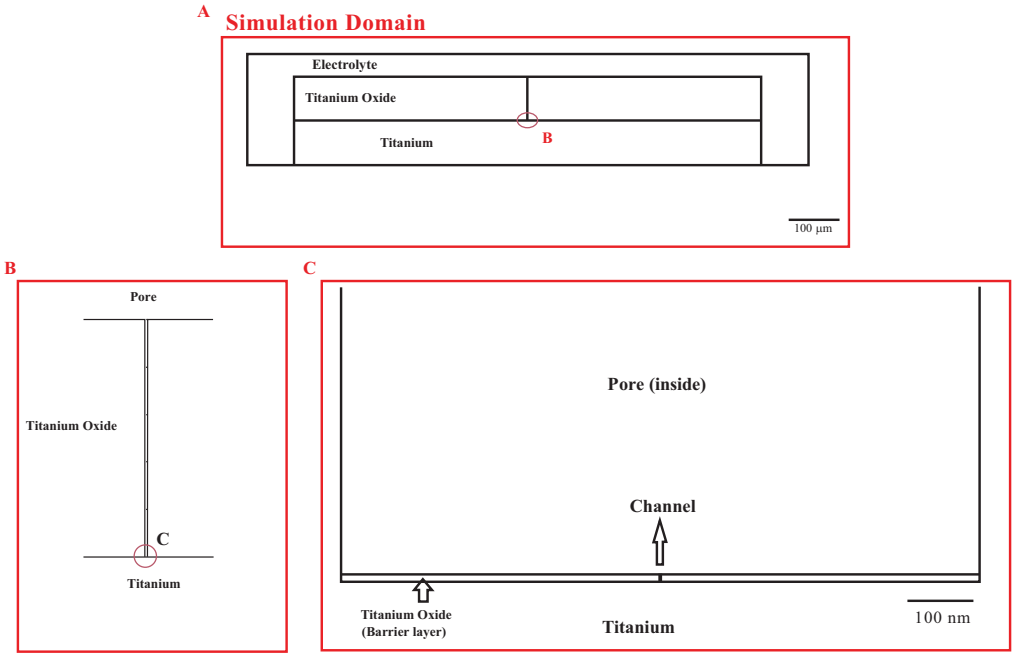

Fig. (3). Domain used to carry out the simulation of the effect of the spark on its surroundings.

of the film, it is possible to conclude that the breakdown event, and hence the spark will occur in the region where the thickness is the smallest. Here we considered this thickness as one of the variables to be investigated, using two different values (10 *nm* and 50 *nm*). We suppose, based on the published papers in the literature [30, 40-43], that the breakdown will generate a channel with high temperatures (5000 K or 10000 K), and with diameter of few nanometers (5 *nm* or 20 *nm*), exposing the metal surface to the solution. Therefore, three different variables are investigated: thickness of the barrier layer, channel diameter and the spark temperature.

The heat influence on the surroundings of the spark was studied through the bi-dimensional Fourier equation (Equation 2). Since the temperature is a function of space and time, the Fourier equation is a partial differential equation that describes the heat distribution by temperature variation over the considered space domain.

$$\frac{\partial T}{\partial t} = \alpha_i \left(\frac{\partial^2 T}{\partial x^2} + \frac{\partial^2 T}{\partial y^2} \right) \frac{\partial T}{\partial t} = \alpha_i \left(\frac{\partial^2 T}{\partial x^2} + \frac{\partial^2 T}{\partial y^2} \right) \quad (2)$$

where, T is the temperature, *x* and y are spatial coordinates, *t* is time and is the thermal diffusion α_i coefficient, which has different values for each considered media. At the external boundary condition, a Dirichlet one using the value of T=300 K was chosen. A Dirichlet condition was also chosen inside the channel, which varies depending on the parameters condition of the theoretical experiment (5000 K or 10000 K). Since we have taken into account the three media involved, the domain also has 3 subdomains, which have the characteristics of each phase considered. These subdomains are in contact with each other. Therefore, in these boundaries, the Dirichlet conditions were not applied, and a continuity condition was used, i.e., $\left(\frac{\partial^2 T}{\partial x^2}\right)_i, \left(\frac{\partial^2 T}{\partial y^2}\right)_i = \left(\frac{\partial^2 T}{\partial x^2}\right)_j, \left(\frac{\partial^2 T}{\partial y^2}\right)_j$, where the indexes *i* and *j* represent the interface of any subdomains in contact.

In order to investigate the effect of the three variables (film thickness, spark temperature and channel diameter) simultaneously, a Factorial Design was used [44]. The Factorial Design is a chemometric tool which can be used to measure the cross effects among the variables besides the main effects. In this method, the total number of experiments (in this case theoretical experiments) to be performed is n^k, where *"n"* is the number of values for each variable and *"k"* is the number of variables. In this work, 3 variables at 2 different levels were investigated, so 2^3=8 experiments were performed. All the conditions of the theoretical experiments carried out are shown in Table **1**.

Considering that a spark is a quantum tunneling phenomenon, its duration time should be extremely short. So, in this simulation a duration time of (t_{spark})= 10^{-9} *s* was considered and as time step in the simulation $\Delta t = 10^{-11}$ *s* was used. According to Matykina *et al.* [19], the life time of a spark is in the range of 35 *ms* up to 800 *ms* depending on the applied voltage. However, we believe those life time results are from 'several sparks' events occurring almost simultaneously with a very short distance between them. As the authors [19] collected their results using a camera with optical zoom of 10 times, it is impossible to acquire all the events with high precision, so the macroscopic answer could be different from what really happens in the "nanoscopic" scale.

One of the characteristic of the finite element method is the division of the domain into small elements, generating a mesh. The mesh for the domain considered in this study is presented in Fig. (**4**). As can be seen, the number of elements increases in the region closest to the boundaries that are subject to Dirichlet condition. The number of elements in the region of interest can be changed into a high value, which refines the mesh. This procedure was used in the breakdown channel region, amplified in Fig. (**4b**), until no changes in

Table 1. Factorial Design 2^3 used to investigate the influence of the variables on the local heating of the film.

Simulation	Thickness (*nm*)	Channel diameter (*nm*)	Temperature (K)
1	10	5	5000
2	50	5	5000
3	10	20	5000
4	50	20	5000
5	10	5	10000
6	50	5	10000
7	10	20	10000
8	50	20	10000

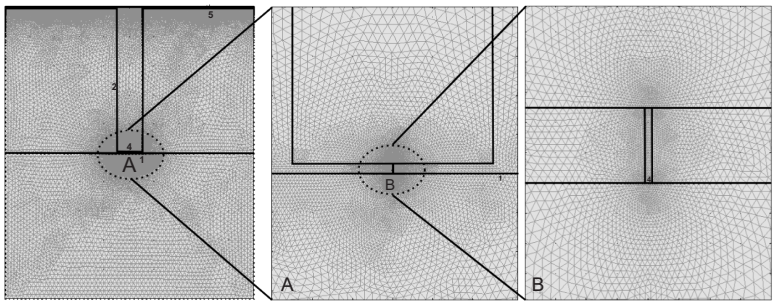

Fig. (4). Refined mesh used to calculate the local heating effect.

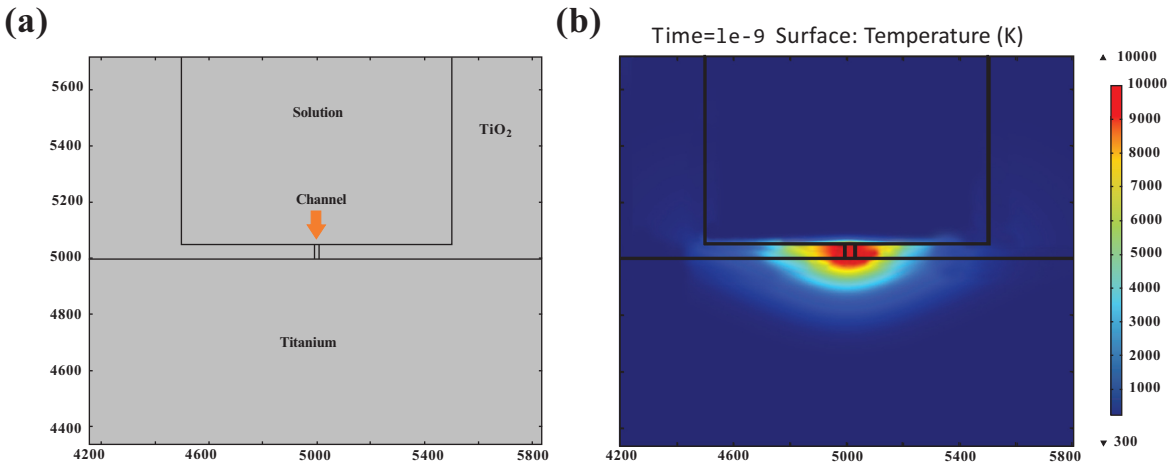

Fig. (5). Domain considered for the condition simulated, and (**b**) Results for the simulation considering T = 10000 K, s = 50 nm and d = 20 nm.

the results were observed. Therefore, the total number of elements in the mesh depends on the conditions used.

RESULTS AND DISCUSSION

Considering the initial conditions described above, the results for the Fourier equation were calculated, which are presented in Fig. (**5**) as a heat distribution over a 2-D space. In this Figure, the variation in color is associated to the changes in the temperature at each point of the domain, which is presented in the side scale of the graphic. As it can be noticed, the heat transfer is higher in the oxide and metal than in the electrolyte. In the solution the heating effect only reaches a small region, which can be neglected compared to the heat released in the oxide and metal subdomains. Analyzing these graphics horizontally, in the region of the channel, a region with higher temperature than the melting temperature of the titanium oxide ($T = 1840\ K$) can be observed, and it is as large as 200 *nm* which is much wider than the channel (5 or 20 nm).

Using the same reasoning as before, but now considering the vertical direction of the channel, it is also possible to observe a significant extension of this region inside the me-

tallic phase which is at a temperature higher than the melting temperature of the titanium (*T=1670 K*). Therefore, according to these results, in the breakdown region, both metal and oxide are viscous fluids, since the temperature is higher than the melting temperature. It is important to stress that such melting is a local effect, which influences just the surrounding region of a spark event. In other words, there is no possibility that the whole material can be liquefied by the temperature increase. However, it can change deeply the properties of the oxide films, such as their morphology and crystallinity.

To quantify the influence of the heat transferred by a spark, the heating radius was regarded as response for this study. Inasmuch as we are interested on the influence of the spark on the properties of the oxide layer, just the heating radius for the oxide was analyzed, the heating radius of the metal being disregarded. As heating radius, a line on the metal/oxide interface was chosen, maintaining the *y* coordinate constant and observing the changes away from the spark event through the *x* coordinate. The size of the radius in the direction *x* was obtained by setting the breakdown channel (i.e., the highest temperature point) as the origin. The radius end was positioned at the point where the temperature is equal to the oxide melting temperature. Therefore, within this radius, we can suppose that all oxide that was previously in the solid phase is now fluid once it melted, and we called this response as "melting radius" (r_M). The curve of *T versus x*, from which the melting radius can be extracted, can be observed in Fig. (**6**). Since the origin of the curve is in the breakdown channel, the temperature decreases as *x* increases. The physical meaning of the melting radius is to demarcate the needed distance for the temperature to fall below the melting temperature of the oxide, which is marked in Fig. (**6**) by the line T_M. This parameter was calculated for all theoretical conditions simulated in Table **1** and the results are shown in Table **2**.

Table **2** presents the results for the melting radius of each simulated condition. As can be seen, when the spark temperature is high, the melting radius also presents high values. The effect of temperature is obvious considering just the heating dissipation process. However, the values in the melting radius, considering the other simulation variables, are not so simple to explain based just on the results presented in Table **2**. Therefore, these data were analyzed using the calculated effects, as shown in Table **3**. It is important to stress out that, in Table **3**, the effects are not the melting radii them-

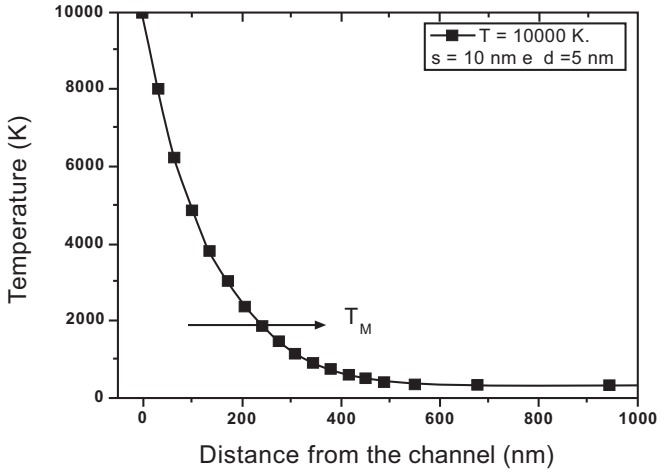

Fig. (6). Temperature *versus* distance from the channel curve for a simulation carried out considering T = 10000 K, *s* = 10 nm and *d* = 5 nm. The melting radius is marked by the line T_M.

Table 2. Melting radius for each condition simulated.

Simulation	Simulation Parameters			Results r_M *(nm)*
	Thickness (*nm*)	Channel diameter (*nm*)	Temperature (K)	
1	10	5	5000	153
2	50	5	5000	269
3	10	20	5000	153
4	50	20	5000	270
5	10	5	10000	238
6	50	5	10000	395
7	10	20	10000	240
8	50	20	10000	394

Table 3. Calculated effects for the melting radius. The relative error associated with the simulation is, ± 0,01.

Mean Value	264
Main Effects	
Thickness	136
Diameter	0.25
Temperature	106
Cross Effect	
Thickness-Diameter	-0.25
Thickness-Temperature	19
Diameter-Temperature	-0.25
Thickness-Diameter-Temperature	-0.75

selves but the changes in their values when the level of each variable is changed.

In the first row of Table **3** the mean value of the melting radius, considering all studied conditions, is presented. In the second row the individual effect of each variable can be seen. As it can be noticed, the thickness and temperature have a strong influence on the size of the melting radius. The value obtained for the thickness, for example, means that, if the thickness of the barrier layer increases from 10 *nm* to 50 *nm*, the melting radius increases to 136 *nm*. This is a change of about 89% if the spark temperature is of 5000 K, and of 57% for the conditions in which the spark temperature was considered to be 10000 K. This observation also shows that there is a cross effect between, at least, two simulation parameters used in this study.

The same behavior is not observed for the diameter of the channel variable. In this case, the change in the value of the channel diameter can be disregarded compared to the influence of the other two variables. So, it is clearly shown that the thickness of the barrier layer and the spark temperature have a stronger influence on the melting radius of the oxide. The temperature effect is obvious since the higher the spark temperature the greater is the dissipation, if the other conditions are kept constant. With the increase in the thickness of the film, there is also an increase in the melting radius, which can be explained by the augment of the heat source area, i.e., the increase of the channel length. Houser and Herbert [29] have shown experimentally that there is a flow of material during the growth of aluminum oxide, however, their supposition about the causes were not discussed in their work. So, here we present a confirmation obtained by a simulation carried out and also a possible explanation for the reasons why the oxide behaves as a Newtonian viscous fluid during the oxide growth.

The results presented in this work supports the conclusion that the mechanism for the crystallization of the film growth by sparking anodization is the local heating caused by the local breakdown in the titanium oxide films. Experimentally, in Fig. (**1**) an increase in the crystalline portion of the films during the sparking anodization was presented. As already discussed, a large number of low intensity sparks were observed in the beginning of the measurements which became more intense with a small number as the anodization continued. Using the simulation results presented here, both situations can be explained by the energy released during the breakdown of the film. According to this line of reasoning, thin films should have a lower crystalline portion than thick films, which is exactly what is observed in the Fig. (**1**), and confirm also the hypothesis already presented in the work of Houser and Herbert [29]. Finally, it was demonstrated that the heating effect of only one spark event occurring in a channel with radius 2.5 nm (5 nm diameter) could reach a radius of 400 nm of the oxide. The ratio of these two variables is 80, but considering the area of the electrode affected by the heat release, the ratio is more than 25,000. This means that a comparatively small number of sparks could melt a much higher amount of the oxide film.

CONCLUSIONS

In this work the influence of the spark on the characteristics of the titanium oxide films has been theoretically investigated by finite element method. The film breakdown can be associated with the emission of sparks when the voltage is high enough. Then, part of the energy stored during the oxide growth is released as heat when the breakdown occurs. This energy generates a local heating of the oxide, promoting its melting in an extension that is dependent on the energy released. Based on this supposition and using some values for the spark temperature experimentally obtained by other authors, we simulated the effect of the spark on the properties of the titanium oxide. In this simulation, using a factorial design approach, the effect of three different parameters: diameter of the breakdown channel, thickness of the barrier layer, and spark temperature was investigated. As a response the melting radius, which is defined as the diameter of the region in the neighbor of a spark in which the temperature reaches a value higher than the melting temperature of the oxide was used. The results have shown that the local heating affects significantly the solid phases involved (metal and oxide). Besides, the thickness of the barrier layer and spark temperature strongly affect the region which is melted immediately after a breakdown event. It was demonstrated that the effect of only one spark event occurring in a channel with radius 2.5 nm (5 nm diameter) could lead to the melting of an area in the oxide which was 25,000 times higher than the channel area. This means that a comparatively small number of sparks could melt a much higher amount of the oxide film.

CONFLICT OF INTEREST

The authors confirm that this article content has no conflict of interest.

ACKNOWLEDGEMENTS

The authors would like to thank the Brazilian research funding agencies CNPq and FAPESP (proc 2008/00180-0) for their financial support. Dr. Mariana de Souza Sikora thanks the colleagues from AMAT for their fruitful discussions.

REFERENCES

[1] Yerokhin, A.L.; Nie, X.; Leyland, A.; Matthews, A.; Dowey, S.J. Plasma electrolysis for surface engineering. *Surf. Coat. Technol.* **1999**, *122*, 73.

[2] Gupta, P.; Tenhundfeld, G.; Daigle, E.O.; Ryabkov, D. Electrolytic plasma technology: Science and engineering--An overview. *Surf. Coatings Technol.,* **2007**, *201*, 8746.

[3] Ma, W.; Wang, S.-H.; Wu, G.-F.; Liu, B.-L.; Wei, J.-H.; Xie, C.; Li, D.-H. Preparation and *in vitro* biocompatibility of hybrid oxide layer on titanium surface. *Surf. Coatings Technol.,* **2010**, *205*, 1736.

[4] Yan, Y.; Sun, J.; Han, Y.; Li, D.; Cui, K. Microstructure and bioactivity of Ca, P and Sr doped TiO_2 coating formed on porous titanium by micro-arc oxidation. *Surf. Coatings Technol.,* **2010**, *205*, 1702.

[5] Casaletto, M.P.; Ingo, G.M.; Kaciulis, S.; Mattogno, G.; Pandolfi, L.; Scavia, G. Surface studies of in vitro biocompatibility of titanium oxide coatings. *Appl. Surf. Sci.,* **2001**, *172*, 167.

[6] Huang, N.; Yang, P.; Leng, Y. X.; Chen, J.Y.; Sun, H.; Wang, J.; Wang, G.J.; Ding, P.D.; Xi, T.F.; Leng, Y. Hemocompatibility of titanium oxide films. *Biomaterials,* **2003**, *24*, 2177.

[7] Kunze, J.; Müller, L.; Macak, J.M.; Greil, P.; Schmuki, P.; Müller, F.A. Time-dependent growth of biomimetic apatite on anodic TiO_2 nanotubes. *Electrochim. Acta,* **2008**, *53*, 6995.

[8] Yetim, A.F. Investigation of wear behavior of titanium oxide films, produced by anodic oxidation, on commercially pure titanium in vacuum conditions. *Surf. Coatings Technol.,* **2010**, *205*, 1757.

[9] Yerokhin, A.L.; Nie, X.; Leyland, A.; Matthews, A. Characterisation of oxide films produced by plasma electrolytic oxidation of a Ti-6Al-4V alloy. *Surf. Coat. Technol.,* **2000**, *130*, 195.

[10] Yerokhin, A.L.; Snizhko, L.O.; Gurevina, N.L.; Leyland, A.; Pilkington, A.; A, M. Discharge characterization in plasma electrolytic oxidation of aluminium. *J. Phys. D. Appl. Phys.,* **2003**, *36*, 2110.

[11] Yerokhin, A.L.; Snizhko, L.O.; Gurevina, N.L.; Leyland, A.; Pilkington, A.; Matthews, A. Spatial characteristics of discharge phenomena in plasma electrolytic oxidation of aluminium alloy. *Surf. Coat. Technol.,* **2004**, *177*, 779.

[12] Wang, L.; Fu, W.; Chen, L. Evolution of active species and discharge sparks in Na2SiO3 electrolyte during PEO process. *J. Alloys Compd.,* **2011**, *509*, 7652.

[13] Wang, L.; Chen, L.; Yan, Z.; Fu, W. Optical emission spectroscopy studies of discharge mechanism and plasma characteristics during plasma electrolytic oxidation of magnesium in different electrolytes. *Surf. Coatings Technol.,* **2010**, *205*, 1651.

[14] Terleeva, O.P.; Belevantsev, V.I.; Slonova, A.I. Types of Discharges in Electrochemical Microplasma Processes. *Prot. Met.,* **2003**, *39*, 50.

[15] Timoshenko, A.V; Magurova, Y.V. Microplasma oxidation of Al-Cu alloys. *Zashchita Met.,* **1995**, *31*, 523.

[16] Albella, J.M.; Montero, I.; Martinez-Duart, J.M. A theory of avalanche breakdown during anodic oxidation. *Electrochim. Acta,* **1987**, *32*, 255.

[17] Di Quarto, F.; Piazza, S.; Sunseri, C. A phenomenological approach to the mechanical breakdown of anodic oxide films on zirconium. *Corros. Sci.,* **1986**, *26*, 213.

[18] Ikonopisov, S. Theory of electrical breakdown during formation of barrier anodic films. *Electrochim. Acta,* **1977**, *22*, 1077.

[19] Matykina, E.; Berkani, A.; Skeldon, P.; Thompson, G.E. Real-time imaging of coating growth during plasma electrolytic oxidation of titanium. *Electrochim., Acta* **2007**, *53*, 1987.

[20] Moon, S.; Jeong, Y. Generation mechanism of microdischarges during plasma electrolytic oxidation of Al in aqueous solutions. *Corros. Sci.,* **2009**, *51*, 1506.

[21] Hussein, R.O.; Nie, X.; Northwood, D.O. Influence of process parameters on electrolytic plasma discharging behaviour and aluminum oxide coating microstructure. *Surf. Coatings Technol.,* **2010**, *205*, 1659.

[22] Sikora, M. de S.; Rosario, A.V.; Pereira, E.C.; Paiva-Santos, C.O. Influence of the morphology and microstructure on the photocatalytic properties of titanium oxide films obtained by sparking anodization in H_3PO_4. *Electrochim. Acta,* **2011**, *56*, 3122.

[23] Leach, J.S.L.; Pearson, B.R. The effect of foreign ions upon the electrical characteristics of anodic ZrO_2 films. *Electrochim. Acta,* **1984**, *29*, 1271.

[24] Vermilyea, D.A. The kinetics of formation and structure of anodic oxide films on tantalum. *Acta Metall.,* **1953**, *1*, 282.

[25] Yahalom, J.; Zahavi, J. Electrolytic breakdown crystallization of anodic oxide films on A1, Ta and Ti. *Electrochim. Acta,* **1970**, *15*, 1429.

[26] Diamanti, M.V; Pedeferri, M.P. Effect of anodic oxidation parameters on the titanium oxides formation. *Corros. Sci.,* **2007**, *49*, 939.

[27] Hussein, R.O.; Nie, X.; Northwood, D.O.; Yerokhin, A.; Matthews, A. Spectroscopic study of electrolytic plasma and discharging behaviour during the plasma electrolytic oxidation (PEO) process. *J. Phys. D-Appl. Phys.,* **2010**, *43*.

[28] Dunleavy, C.S.; Golosnoy, I.O.; Curran, J.A.; Clyne, T.W. Characterisation of discharge events during plasma electrolytic oxidation. *Surf. Coatings Technol.,* **2009**, *203*, 3410.

[29] Houser, J.E.; Hebert, K.R. The role of viscous flow of oxide in the growth of self-ordered porous anodic alumina films. *Nat. Mater.,* **2009**, *8*, 415.

[30] Habazaki, H.; Onodera, T.; Fushimi, K.; Konno, H.; Toyotake, K. Spark anodizing of [beta]-Ti alloy for wear-resistant coating. *Surf. Coatings Technol.,* **2007**, *201*, 8730.

[31] Song, H.-J.; Kim, M.-K.; Jung, G.-C.; Vang, M.-S.; Park, Y.-J. The effects of spark anodizing treatment of pure titanium metals and titanium alloys on corrosion characteristics. *Surf. Coatings Technol.,* **2007**, *201*, 8738.

[32] Monfort, F.; Matykina, E.; Berkani, A.; Skeldon, P.; Thompson, G. E.; Habazaki, H.; Shimizu, K. Species separation during coating growth on aluminium by spark anodizing. *Surf. Coatings Technol.,* **2007**, *201*, 8671.

[33] COMSOL Multiphysics.

[34] Parkhutik V.P.; Albella, J.M.; Martinez.-Duart. J.M. In: *Modern Aspects of Electrochemistry*; Conway, B.E., White, J., Bockris, J.O.M. Ed.; Plenum Press: New York, 1992.

[35] Foca, E.; Carstensen, J.; Foll, H. Modelling electrochemical current and potential oscillations at the Si electrode. *J. Electroanal. Chem.* **2007**, *603*, 175.

[36] Foll, H.; Carstensen, J.; Foca, E. Self-induced oscillations in Si and other semiconductors. *Int. J. Mater. Res.,* **2006**, *97*, 1016.

[37] Carstensen, J.; Prange, R.; Popkirov, G.S.; Föll, H. A model for current oscillations in the Si-HF system based on a quantitative analysis of current transients. *Appl. Phys. A Mater. Sci. Amp; Process.,* **1998**, *67*, 459.

[38] Foll, H.; Leisner, M.; Cojocaru, A.; Carstensen, J. Self-organization phenomena at semiconductor electrodes. *Electrochim. Acta,* **2009**, *55*, 327.

[39] Logan, D.L. *A First Course in the Finite Element Method*; 4th ed.; Thomson: Toronto, **2007**.

[40] Klapkiv, M.D. Simulation of synthesis of oxide-ceramic coatings in discharge channels of a metal-electrolyte system. *Mater. Sci.,* **1999**, *35*, 279.

[41] Klapkiv, M.D.; Povstyana, N.Y.; Nykyforchyn, H.M. Production of conversion oxide-ceramic coatings on zirconium and titanium alloys. *Mater. Sci.,* **2006**, *42*, 277.

[42] Krupa, D.; Baszkiewicz, J.; Zdunek, J.; Smolik, J.; Slomka, Z.; Sobczak, J.W. Characterization of the surface layers formed on titanium by plasma electrolytic oxidation. *Surf. Coatings Technol.,* **2010**, *205*, 1743.

[43] Dunleavy, C.S.; Curran, J.A.; Clyne, T.W. Self-similar scaling of discharge events through PEO coatings on aluminium. *Surf. Coat. Technol.,* **2011**, *206*, 1051.

[44] Bruns, R.E.; Scarminio, I.S.; Neto, B. de B. Statistical Design - Chemometrics, (Data Handling in Science and Technology); Elsevier Science, **2006**; Vol. *25*, p. 422.

Received: November 19, 2014 Revised: December 23, 2014 Accepted: January 18, 2015